LEWIS GRANT
IN-25-CR
135352
24p.

THE OHIO STATE UNIVERSITY

Material Parameter Measurements at High Temperatures

by

A. Dominek, A. Park and L. Peters, Jr.

The Ohio State University

ElectroScience Laboratory

Department of Electrical Engineering
Columbus, Ohio 43212

(NASA-CR-182707) MATERIAL PARAMETER MEASUREMENTS AT HIGH TEMPERATURES (Ohio State Univ.) 24 p CSCL 07D

N88-20357

Unclas
G3/25 0135352

Technical Report No. 719300-2
Grant No. NAG3-784
March 1988

National Aeronautics and Space Administration
Lewis Research Center
21000 Brookpark Rd.
Cleveland, OH 44135

50272-101

REPORT DOCUMENTATION PAGE	1. REPORT NO.	2.	3. Recipient's Accession No

4. Title and Subtitle

Material Parameter Measurements at High Temperatures

5. Report Date
March 1988

6.

7. Author(s)
A. Dominek, A. Park and L. Peters, Jr.

8. Performing Organization Rept. No

9. Performing Organization Name and Address
The Ohio State University
ElectroScience Laboatory
1320 Kinnear Road
Columbus, Ohio 43212

10. Project/Task/Work Unit No
719300-2

11. Contract(C) or Grant(G) No
(C)
(G) NAG3-784

12. Sponsoring Organization Name and Address
National Aeronautics and Space Administration
Lewis Research Center
21000 Brookpark Road
Cleveland, Ohio 44135

13. Type of Report & Period Covered
Technical

14

15. Supplementary Notes

16. Abstract (Limit: 200 words)

Alternate fixtures of techniques for the measurement of the constitutive material parameters at elevated temperatures are presented. The technique utilizes scattered field data from material coated cylinders between parallel plates or material coated hemispheres over a finite size ground plane. The data acquisition is centered around the HP 8510B Network Analyzer. The parameters are then found from a numerical search algorithm using the Newton-Raphson technique with the measured and calculated fields from these canonical scatterers. Numerical and experimental results are shown.

17. Document Analysis a. Descriptors

b. Identifiers/Open-Ended Terms

c. COSATI Field/Group

18. Availability Statement	19. Security Class (This Report)	21. No. of Pages
	Unclassified	20
	20. Security Class (This Page) Unclassified	22. Price

(See ANSI-Z39.18) See Instructions on Reverse OPTIONAL FORM 272 (4-77) (Formerly NTIS-35) Department of Commerce

Contents

List of Figures iv

1 Introduction 1

2 Alternate Measurement Fixtures 3

3 Parameter Extraction 7

4 Canonical Sample Geometries 10

5 Example Calculations 14

6 Conclusions 19

PRECEDING PAGE BLANK NOT FILMED

PAGE ii INTENTIONALLY BLANK

List of Figures

2.1 Illustration of the parallel plate test fixture. 4

2.2 Illustration of the ogival shaped ground plane test fixture. . 6

4.1 Geometry for a coated cylinder. 11

4.2 Geometry for a coated hemisphere. 13

5.1 Echo widths for circular cylinders. Perfectly conducting - solid, homogeneous dielectric - short dashed and coated - long dashed. Perfectly conducting and coated cylinder results are very similar for these parameters. 15

5.2 Echo areas for hemispheres on an infinite ground plane. Perfectly conducting - solid, homogeneous dielectric - short dashed and coated - long dashed. 16

5.3 Sphere diameter sensitivity example to estimate the relative permittivity from calculated values based upon a diameter of 3" and relative permittivity of 2.6. Assumed diameter: 3" - Solid, 2.97" - dot-dashed and 3.03" - short dashed. 17

5.4 Numerically determined relative permittivity from measured backscattered data for a 3" diameter sphere. 18

Chapter 1

Introduction

Conventional techniques for the evaluation of the constitutive material parameters involves material samples filling an interior region of a coaxial or waveguide line. Care must be exercised in acquiring the sample to insure a firm fit in the line to obtain accurate reflection and transmission measurements. The use of such a line fixture to perform these measurements becomes undesirable at high temperatures (greater than 800° F) due to mechanical and electrical considerations of the line. Alternate approaches are suggested here to eliminate the need of closed system measurements to acquire material parameters. The upper temperature restriction in these approaches would be limited by the fixture durability and the means to generate the desired temperatures within these fixtures. The alternate system involves the measurement of scattered fields from canonical sample geometries using parallel plate or ground plane fixtures. The material parameters can then be found from measurements and exact numerical expressions for the scattered fields from these sample canonical geometries. Similar free space measurements have been performed for material coated plates based upon a reflection model [2].

The swept frequency measurements acquired with either of these fixtures can readily be performed with the HP 8510B Network Analyser. The software time gating of the HP 8510B would be implemented to eliminate

error terms from the edge scattering of the finite fixture size.

Chapter 2

Alternate Measurement Fixtures

There are two possible fixtures that would readily allow the necessary scattered field measurements from heated sample geometries. They are a parallel plate and ground plane geometries shown in Figures 2.1 and 2.2, respectively. The canonical sample geometries used in these fixtures are circular cylinders for the parallel plate fixture and hemispheres for the ground plane fixture. These geometries are the most natural because their exact scattered fields are readily computed from eigenfunction solutions for either homogeneous material geometries or material coated perfectly conducting geometries.

The parallel plate geometry is ideal for low frequency measurements where the wavelength of the incident frequency is greater than twice the distance between the parallel sides of the fixture. This restriction is so that only one dominant mode exists in the fixture. It is suggested that the material sample be coated on a hollow perfectly conducting cylinder to allow internal heating by an electric or gas source. This internal heating approach would eliminate possible mechanical and electrical difficulties caused by a heat source in between the parallel plates. For the heat source between the parallel plates, the sample would have to be rotated to insure uniform heating. The difficulty arises from the crack that would be formed to allow

the rotation. The scattering from the crack would have to be accounted for in the analytic model which would be difficult. The rotation of the sample would also have to be very uniform along its axis. Another benefit of internal sample heating is that no consideration is required for the scattering from the heat source. Permitting the heat source between the parallel plates would introduce another timing constraint for the separation distance between the sample and heat source. The expansion of the sample due to the heat is of no great concern as long as it is known for the parameter determination. It is necessary however to maintain tight contact between the sample and the sides of the parallel plates.

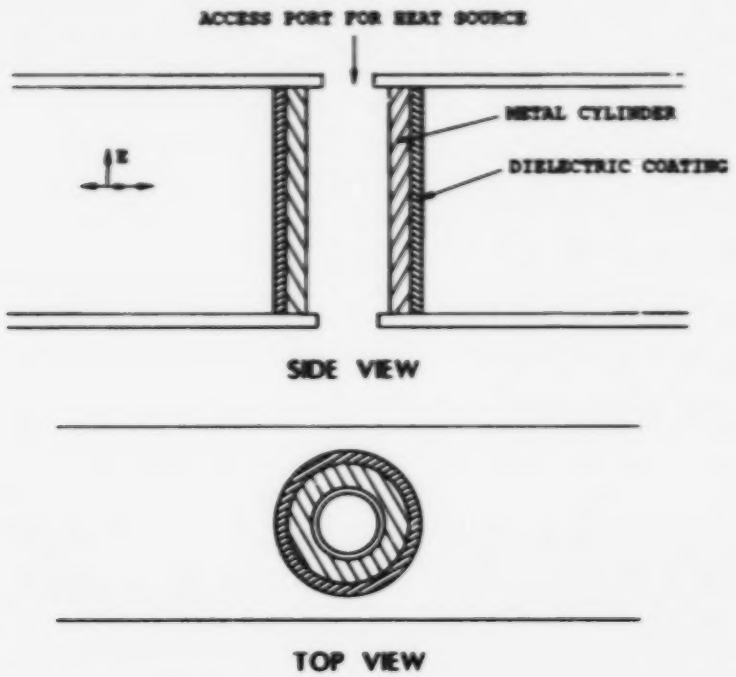

Figure 2.1: Illustration of the parallel plate test fixture.

Many of the same concepts for the parallel plate fixture are applicable to the ground plane fixture. Again it would be desirable to heat the sample internally to exclude scattering from the heat source and the crack in the ground plane which would permit rotation. It would be very desirable to

shape the ground plane to have an ogival contour to control the scattered field from its edges. The heating hardware would have to be shielded by extending a curved metal surface from the ground plane surface.

It is important that the distance between the test sample and the source be large enough to produce a planar illuminating field for the test sample. This is for a simplification of the calculation of the exact scattered fields, though it is not absolutely necessary. This minimal distance, called the range distance R, is given by

$$R = 2\frac{\ell^2}{\lambda}$$

where ℓ is the maximum length of the test sample geometry and λ is the wavelength of the incident field [1]. The maximum phase variation of the incident wavefront at this distance is 22.5°.

The range distance is not the dominating factor for the parallel plate fixture if the upper frequency is set at 18 GHz. The distance between the parallel plates for only the dominant mode to exist is approximately .325 inches. The main test bed of the parallel plate fixture should be at least 1.5 feet square with the sample in the middle. The fixture requires a feed region that would consist of a tapered parallel plate geometry expanding from a vertex feed to the width of the main fixture. The length of the feed should be approximately 1.5 feet long. This fixture would be very desirable in terms of providing a uniform, high temperature environment to the sample. The major disadvantage for this fixture is that the material sample length could be too short for an adequate field interaction to occur.

The minimal range distance for the ground plane fixture is 5 meters if an upper frequency of 18 GHz is desired. A tip to tip length for the ground plane should be in the vicinity of 6 feet with a ground plane width of 1 foot.

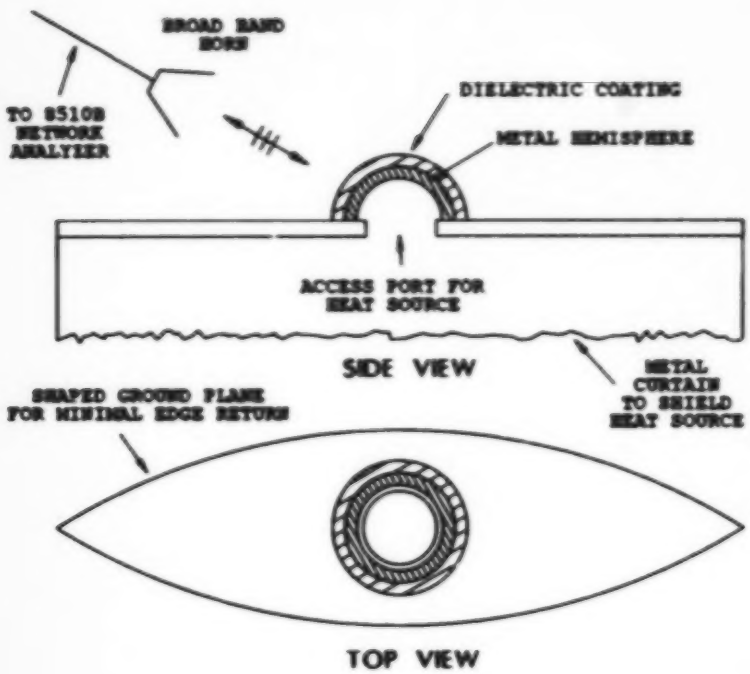

Figure 2.2: Illustration of the ogival shaped ground plane test fixture.

Chapter 3

Parameter Extraction

Extracting the constitutive parameters from measured swept frequency data requires two items. One item is calibrated data and the other is an exact solution for the measured scattered field. Calibrated data is obtained from three measurements, these being test sample data, background data (no test sample present) and data from a known reference. This data is then used in the following formula to obtain calibrated data

$$\mathrm{CSD} = \left(\frac{\mathrm{MSD} - \mathrm{MBD}}{\mathrm{MRD} - \mathrm{MBD}}\right) \mathrm{CRD} \tag{3.1}$$

where CSD is calibrated sample data, MSD is measured sample data, MBD is measured background data, MRD measured reference data and CRD is calculated (exact) reference data. The vector subtraction using the measured background is not necessary if stray scattered signals are negligible or the HP 8510B Network Analyzer time gating window is small enough to include only the desired signal.

Once the measured data has been calibrated, the Newton-Raphson technique can be applied to numerically search for the proper constitutive parameters of the material, ε and μ. Since these parameters are complex, two independent measurements have to be performed. In cases where the parameters are not highly sensitive to frequency, two measurements at slightly different frequencies will suffice or an average of values around the frequency

of interest will also work [2]. Such an approach has to be taken for monostatic (transmitting and receiving horns are at the same location) scattering measurements using the parallel plate fixture. Independent measurements at the same frequency for this fixture can be obtained if bistatic measurements are taken. The ground plane fixture has two extra features available for independent measurements which are the polarization of the incident field and the elevation angle of the incident field direction from the ground plane surface.

Another potential means to obtain independent scattered field relationships from one measurement is to isolate the individual scattering mechanisms that occur in the total scattered field. The scattered field for a homogeneous dielectric sphere has several wave interactions. The two most apparent ones are the reflection from the front surface and the internal reflection from the rear surface. These two reflections are dependent upon the constitutive parameters in different functional relationships. Effectively two different measurements can be obtained from one measurement if these reflections are separated in time enough so they can be isolated from the total scattered field by the time gating software in the HP 8510B.

The Newton-Raphson technique iteratively solves for the unknown parameters by forcing two convenient functionals to zero. Defining the functionals, $F_{0,1}$, to be

$$F_0 = M_0 - C_0 = 0 \tag{3.2}$$

and

$$F_1 = M_1 - C_1 = 0 \tag{3.3}$$

where the $M_{1,2}$ and $C_{1,2}$ are the independent measured and calculated responses for the sample geometry. The calculated responses are dependent

upon the parameters ϵ and μ which are iteratively varied until some minimum error criterion has been achieved. The unknown parameters are iterated with the following process from some initial guess

$$\epsilon_{i+1} = \epsilon_i + \Delta\epsilon_i \tag{3.4}$$

and

$$\mu_{i+1} = \mu_i + \Delta\mu_i \tag{3.5}$$

where

$$\Delta\epsilon = \frac{F_1 \frac{\partial F_0}{\partial \epsilon} - F_0 \frac{\partial F_1}{\partial \epsilon}}{J} \tag{3.6}$$

and

$$\Delta\mu = \frac{F_0 \frac{\partial F_1}{\partial \mu} - F_1 \frac{\partial F_0}{\partial \mu}}{J} \tag{3.7}$$

and

$$J = \begin{vmatrix} \frac{\partial F_0}{\partial \epsilon} & \frac{\partial F_0}{\partial \mu} \\ \frac{\partial F_1}{\partial \epsilon} & \frac{\partial F_1}{\partial \mu} \end{vmatrix}. \tag{3.8}$$

Chapter 4

Canonical Sample Geometries

The exact scattered fields for the canonical sample geometries are readily calculated by eigenfunction expressions. The geometry for a coated perfectly conducting circular cylinder is shown in Figure 4.1. The scattered far field for plane wave illumination is given by [3]

$$E_z^s = E_z^i \sqrt{\frac{2}{\pi}} e^{j\frac{\pi}{4}} \frac{e^{-jk\rho}}{\sqrt{k\rho}} \sum_{n=0}^{\infty} a_n \cos n(\frac{\pi}{2} - \phi) \tag{4.1}$$

where a_n are ratios of cylindrical Bessel functions, J_n, N_n and $H_n^{(2)}$ and given by

$$a_n = -\epsilon_n \frac{J_n'(kb) - Z_n J_n(kb)}{H_n^{(2)\prime}(kb) - Z_n H_n^{(2)}(kb)} \tag{4.2}$$

and

$$Y_n = \eta_r^{-1} \frac{J_n(k_1 a) N_n'(k_1 b) - N_n(k_1 a) J_n'(k_1 b)}{J_n(k_1 a) N_n(k_1 b) - N_n(k_1 a) J_n(k_1 b)} \tag{4.3}$$

where $\eta_r = \sqrt{\frac{\mu_r}{\epsilon_r}}$ is the relative wave impedance of the material and $k_1 = \sqrt{\epsilon_r \mu_r} k$ and k is the free space wave number. The parameter ϵ_n is equal to unity for $n = 0$ and 2 for $n \neq 0$.

These above expressions reduce to simpler forms for special cases. The quantity Y_n is equal to

$$\eta_r^{-1}\frac{J_n'(k_1 b)}{J_n(k_1 b)}$$

for a homogeneous cylinder. Additionally, for the perfectly conducting cylinder, $Y_n = \infty$.

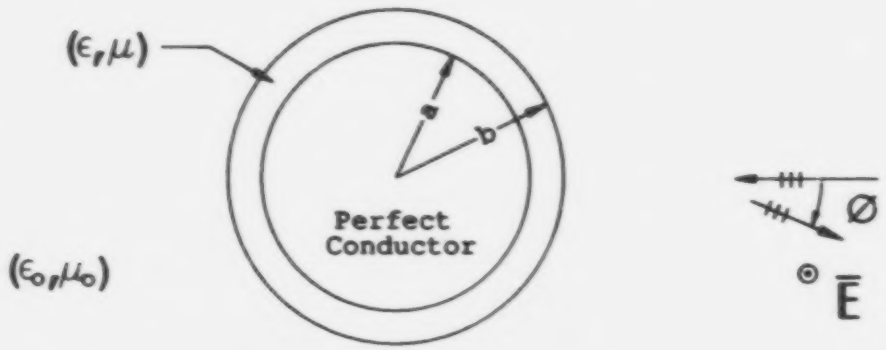

Figure 4.1: Geometry for a coated cylinder.

The geometry of a coated perfectly conducting hemisphere over an infinite ground plane is shown in Figure 4.2. The scattered far field for plane wave illumination can be calculated by using image theory which results in the sum of the backscattered and bistatic scattered fields for a sphere in free space. The scattered field for a hemisphere on a ground plane can be written in the following form for the two principal polarizations

$$E_\theta = E_\theta^{sphere}(\theta = 0) + E_\theta^{sphere}(\theta = 2\theta_0) \tag{4.4}$$

and

$$E_\phi = E_\phi^{sphere}(\theta = 0) - E_\phi^{sphere}(\theta = 2\theta_0) \tag{4.5}$$

where $E_{\theta,\phi}^{sphere}$ is the scattered field for a sphere in free space at a bistatic angle of θ_0.

The scattered field expressions for a sphere in free space are given by [3]

$$E_\theta^{sphere}(\theta) = -j\frac{E_o}{kr}e^{-jkr}\sum_{n=1}^{\infty}\left[b_n \sin\theta P_n^{1\prime}(\cos\theta) - c_n\frac{P_n^1(\cos\theta)}{\sin\theta}\right] \qquad (4.6)$$

and

$$E_\phi^{sphere}(\theta) = -j\frac{E_o}{kr}e^{-jkr}\sum_{n=1}^{\infty}\left[b_n\frac{P_n^1(\cos\theta)}{\sin\theta} - c_n \sin\theta P_n^{1\prime}(\cos\theta)\right] \qquad (4.7)$$

where $P^1(\cos\theta)$ and $P^{1\prime}(\cos\theta)$ are Legendre polynomials and

$$b_n = b_n^\circ\frac{B_n(A_nF_n^1 - \eta_r X_n F_n^2)}{A_n(B_nF_n^1 - \eta_r X_n F_n^2)} \qquad (4.8)$$

and

$$c_n = c_n^\circ\frac{(X_nF_n^3 - \eta_r A_n F_n^4)}{(X_nF_n^3 - \eta_r B_n F_n^4)}. \qquad (4.9)$$

where $\eta_r = \sqrt{\frac{\mu_r}{\epsilon_r}}$ is the relative wave impedance of the material. The symbols b_n°, c_n°, A_n, B_n, X_n and $F_n^{1,2,3,4}$ are ratios of spherical Bessel functions j_n and h_n given by

$$b_n^\circ = -\frac{2n+1}{n(n+1)}\frac{[kbj_n(kb)]'}{\left[kbh_n^{(2)}(kb)\right]'}, \qquad (4.10)$$

$$c_n^\circ = -\frac{2n+1}{n(n+1)}\frac{j_n(kb)}{h_n^{(2)}(kb)}, \qquad (4.11)$$

$$A_n = \frac{[kbj_n(kb)]'}{kbj_n(kb)} \qquad (4.12)$$

$$B_n = \frac{\left[kbh_n^{(2)}(kb)\right]'}{kbh_n^{(2)}(kb)} \qquad (4.13)$$

$$X_n = \frac{[k_1 b j_n(k_1 b)]'}{k_1 b j_n(k_1 b)} \tag{4.14}$$

$$F_n^1 = 1. - \frac{[k_1 a j_n(k_1 a)]'}{j_n(k_1 b)} \frac{h_n^{(2)}(k_1 b)}{\left[k_1 a h_n^{(2)}(k_1 a)\right]'}, \tag{4.15}$$

$$F_n^2 = 1. - \frac{[k_1 a j_n(k_1 a)]'}{[k_1 b j_n(k_1 b)]'} \frac{\left[k_1 b h_n^{(2)}(k_1 b)\right]'}{\left[k_1 a h_n^{(2)}(k_1 a)\right]'}, \tag{4.16}$$

$$F_n^3 = 1. - \frac{j_n(k_1 a)}{[k_1 b j_n(k_1 b)]'} \frac{\left[k_1 b h_n^{(2)}(k_1 b)\right]'}{h_n^{(2)}(k_1 a)} \tag{4.17}$$

and

$$F_n^4 = 1. - \frac{j_n(k_1 a)}{j_n(k_1 b)} \frac{h_n^{(2)}(k_1 b)}{h_n^{(2)}(k_1 a)} \tag{4.18}$$

where $k_1 = \sqrt{\epsilon_r \mu_r} k$ and k is the free space wave number.

These above expressions also reduce to simpler forms for special cases. The $F_n^{1,2,3,4}$ quantities are equal to unity for a homogeneous sphere. Additionally, for the perfectly conducting sphere, $b_n = b_n^o$ and $c_n = c_n^o$.

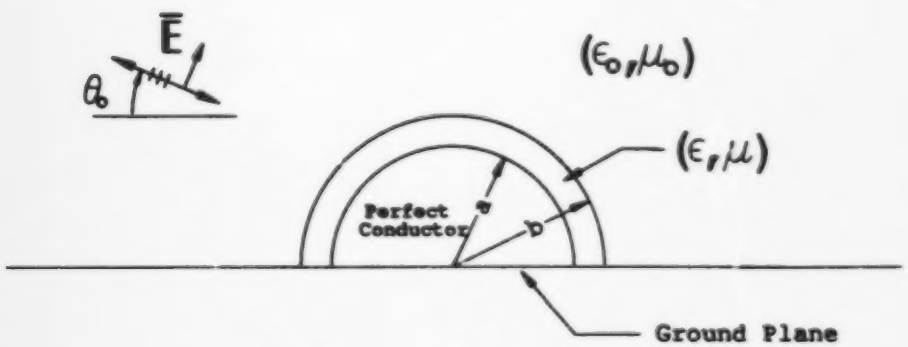

Figure 4.2: Geometry for a coated hemisphere.

Chapter 5

Example Calculations

The examples that follow have been chosen for simplicity and ease of computation to illustrate the concepts involved. The thin material coatings are lossless with $\mu_r = 1.0$. Obviously the introduction of thicker, lossy coatings with $\mu_r \neq 1.0$ will increase the influence of the material on the scattered fields from the conducting surfaces. These solutions should be carried to a conclusion in further studies in a manner similar to the work of Yu and Peters [4].

The backscattered fields of the canonical geometries are calculated for comparison purposes between the perfectly conducting case, the homogeneous dielectric case and the dielectric coated-perfectly conducting case. The calculated fields are expressed as echo widths for the circular cylinder geometries, given by

$$\sigma_W = 2\pi \lim_{\rho \to \infty} \left| \frac{E^s}{E^i} \right|^2, \tag{5.1}$$

and echo areas for the hemispherical geometries, given by

$$\sigma_A = 4\pi \lim_{r \to \infty} \left| \frac{E^s}{E^i} \right|^2 \tag{5.2}$$

where $E^{s,i}$ are the scattered and incident electric fields. Figure 5.1 shows the echo widths for a 2" diameter perfectly conducting circular cylinder, 2"

diameter dielectric circular cylinder with $\epsilon_r = 2.6$ and a coated 2" diameter perfectly conducting circular cylinder with a coating thickness of .04" and $\epsilon_r = 2.6$ calculated between 2 and 18 GHz. In this case, the coating for its electrical thickness and constitutive parameters has negligible influence on the scattered fields in this frequency range. Its scattered fields for the coated case are essentially the same as the perfectly conducting case. Figure 5.2 shows the echo widths for a 3" diameter perfectly conducting hemisphere, 3" diameter dielectric hemisphere with $\epsilon_r = 2.6$ and a coated 3" diameter perfectly conducting hemisphere with a coating thickness of .04" and $\epsilon_r = 2.6$ calculated between 2 and 18 GHz. In all calculations, $\mu_r = 1$.

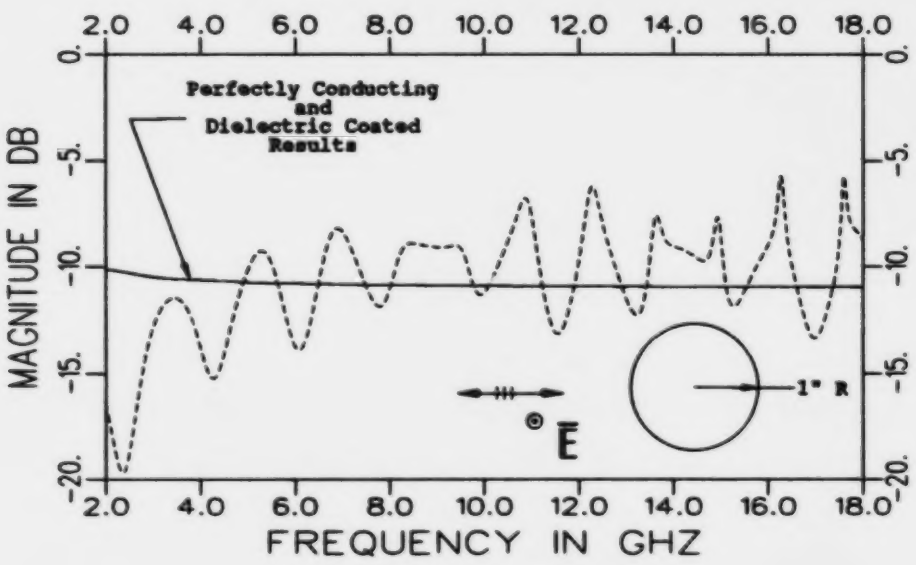

Figure 5.1: Echo widths for circular cylinders. Perfectly conducting - solid, homogeneous dielectric - short dashed and coated - long dashed. Perfectly conducting and coated cylinder results are very similar for these parameters.

These figures readily illustrate the minor influence the material coating has on the scattered fields when the material parameters are not significantly different from free space. The influence of the coating becomes more pronounced with thicker electrical coatings. The homogeneous dielectric

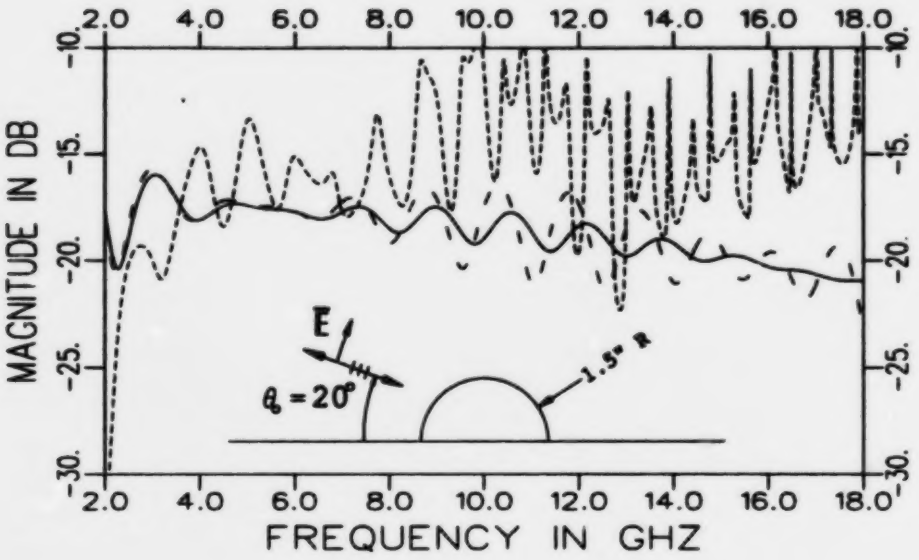

Figure 5.2: Echo areas for hemispheres on an infinite ground plane. Perfectly conducting - solid, homogeneous dielectric - short dashed and coated - long dashed.

cases do not have this limitation due to the absence of the inner conducting core.

A sensitivity study was performed on a numerical technique to extract the relative permittivity, ε_r from calculated backscattered fields from a 3" diameter homogeneous dielectric sphere with $\varepsilon_r = 2.6$. A functional similar to that described earlier was used except calculated data was used instead of measured data. Figure 5.3 shows the calculated relative permittivity assuming the sphere diameter to be 2.97", 3.0" and 3.03". A 1% change in the assumed sphere diameter created approximately a 2% error in the calculated relative permittivity.

The final example is the determination of the relative permittivity of a relatively lossless 3" dielectric sphere from backscattered measurements. Figure 5.4 shows the results between 2 and 10 GHz. A value of $\varepsilon_r = 2.6$

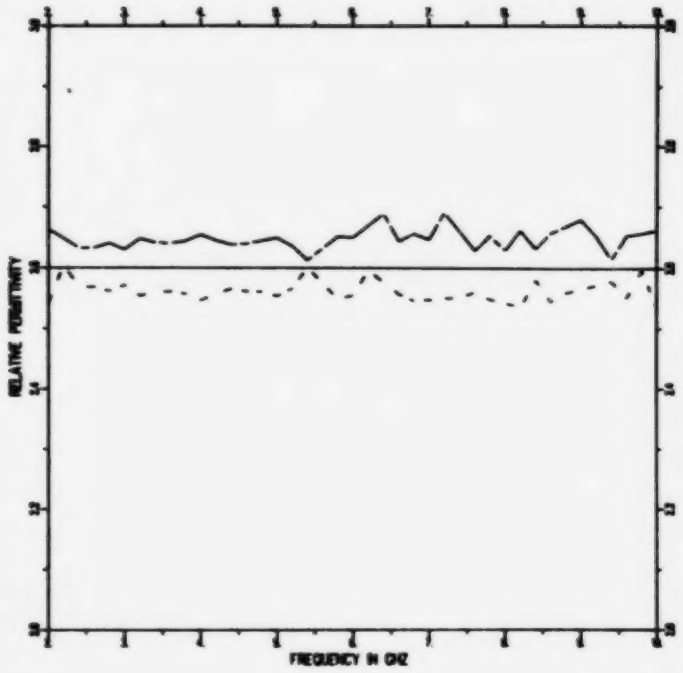

Figure 5.3: Sphere diameter sensitivity example to estimate the relative permittivity from calculated values based upon a diameter of 3" and relative permittivity of 2.6. Assumed diameter: 3" - Solid, 2.97" - dot-dashed and 3.03" - short dashed.

was obtained which is reasonable for the material.

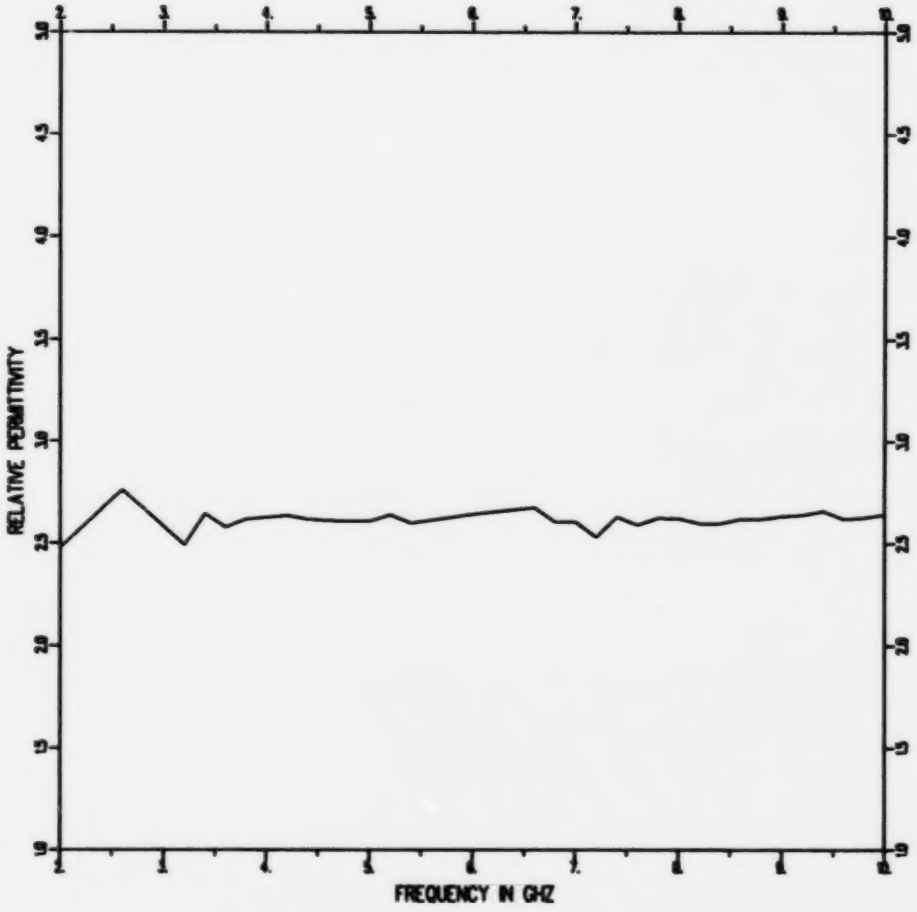

Figure 5.4: Numerically determined relative permittivity from measured backscattered data for a 3" diameter sphere.

Chapter 6

Conclusions

The constitutive parameters can be obtained in principle from scattered field measurements of a material body. The ground plane fixture required for such a technique does not involve the temperature related difficulties which the traditional technique for material parameter measurements has. Of the two scatterers examined, the hemispherical geometry is more desirable in terms of fixture design and electrical performance. The most reliable parameter determination from measured scattered fields of a material coated, perfectly conducting scatterer is obtained with electrically thick coatings.

Bibliography

[1] Kouyoumjian, R.G. and L. Peters, Jr., "Range Requirements in Radar Cross-Section Measurements," IEEE Proc. Vol. 53, No. 8, pp. 920-928, August 1965.

[2] Walton, E.K., M. Mittal, R. Slyh, and M. Poirier, "Development of an Advanced Microwave Free-Space Material Measurement System," ElectroScience Laboratory, Report No. 529696-1, July 1986.

[3] Swarner, W.G., "Radar Cross Sections of Dielectric or Plasma Coated Conducting Bodies," ElectroScience Laboratory, Report No. 1116-21, August 1962.

[4] Yu, J.S. and L. Peters, Jr., "Measurement of Constitutive Parameters Using the Mie Solution of a Scattering Sphere," IEEE Proc., Vol. 58, No. 6, pp. 876-85, June 1970.